Seventh International Conference on CFD in the Minerals and Process Industries
CSIRO, Melbourne, Australia
9-11 December 2009

MODELLING VARIATIONS IN SHEAR RATE AROUND A GEOMETRICALLY SIMILAR THROMBUS *IN-VITRO*

Christopher J. BUTLER, Gregory J. SHEARD and Kris RYAN

Department of Mechanical and Aerospace Engineering, Monash University, Victoria 3800, AUSTRALIA

ABSTRACT

The flow of blood past an axisymmetric thrombus in an *in-vitro* geometry is computed through the solution of the three-dimensional (3D) Navier-Stokes equations. A spectral-element solver coupled with an azimuthal Fourier expansion forms the 3D spatial discretisation scheme. Particle tracking is used to simulate the flow of thrombocytes (platelets) through the geometry at appropriate distances from the wall. The thrombus is shown to experience significant increases in local shear rate (up to 300%) over the Poiseuille flow conditions. A significant variation in both the maximum shear rate achieved in the vicinity of the thrombus, and the local shear behaviour, is observed as the thrombus increases in size within the channel.

NOMENCLATURE

AR	Aspect ratio
H	Depth of channel
V	Derivative tensor
H_T	Height of thrombus
h_T	Nondimensional thrombus height
L	Radial size of mesh
P	Kinematic pressure
S	Strain tensor
r_T	Radius of curvature of the thrombus
γ	Shear rate
$\mathbf{u}$	Velocity (vector form)
τ	Shear force
λ	Principal strains
χ	Normalized shear
υ	Kinematic viscosity

INTRODUCTION

Heart disease is the leading cause of death in Australia and many Western nations. Heart disease is a generic term covering a multitude of cardio-vascular diseases and disorders which can range in severity from mild to fatal. Studies have long shown that there are flow dependent effects on the vascular system (Caro et al., 1969) particularly regarding thrombosis. Thrombosis is the process of occlusion of vascular vessels via the formation of a blood clot (a thrombus). Thrombosis is commonly associated with stroke and heart disease (Wootton and Ku, 1999). In general, a thrombus is an aggregate of blood cells and proteins which bond together at an injury site on a blood vessel wall. The thrombus structure is dominated by bonding between platelets and the appropriate proteins. As a result, the activation and adherence of platelets is a critical factor in the formation of a thrombus (Eisenberg and Ghigliotti, 1999). An important question may be posed; after forming an initial thrombus structure at the site of vessel wall damage, what interactions mediate platelet aggregation, adhesion and activation after the isolation of the injury site from the flow (Hathcock, 2006)? These processes may be triggered by a variety of chemical agonists (Wootton and Ku, 1999). However, biomechanical interactions, particularly the effect of shear forces to which the platelets are exposed to are thought to affect platelet-thrombus interactions (Kroll et al., 1996).

The interaction of these processes is complex, yet recent studies have shown that the initial tether formation between platelets and the adhering surfaces are shear rate (γ) dependent (Dopheide et al., 2002; Maxwell et al., 2007). Additionally Gonclaves et al. (2005) showed temporal variations in shear affect the activation rate of platelets. The shear environment in these papers was controlled by using micro-slides to form a perfusion channel. Recent work such as Tolouei et al. (2008) and Nesbitt et al. (2009) has placed heavy emphasis on the fact that variations in shear occur around thrombotic growths in these channels. Additionally artificial disturbances in shear introduced into the channel in Nesbitt et al (2009) were shown to trigger platelet aggregation. The aggregation was attributed to spatial "micro gradients" in shear rate. It was noted (Fouras, 2008) that these thrombi reach a steady state size within the perfusion channel, suggesting a change in shear behaviour may occur during thrombus growth.

This study seeks to model a thrombus in a perfusion channel by matching the experiments of Tolouei et al. (2008) and Nesbitt et al. (2009); paying particular attention to the changes in behaviour of the shear forces both on and in the local vicinity of a thrombus as it gets larger within the channel. Attention is to be payed to the effect the variation of thrombus height has on the shear rate maximum as well as the spatial and temporal gradients of shear rate.

MODEL DESCRIPTION

The model and parameters established for this study are based on the two papers stated in the introduction. These papers considered *in-vitro* geometries, due to the lack of control provided by *in-vivo* systems. As a result this study models the experimental geometries where the biochemical effects are tightly controlled. The geometry of the thrombus is axisymmetric in shape and geometrically similar as it grows in the channel. We note at this stage that the experimental studies use a chemical

agonist to stimulate the initial formation of the thrombus. As a result of this control, the thrombus can be considered to always be adhered to the lower surface of the channel.

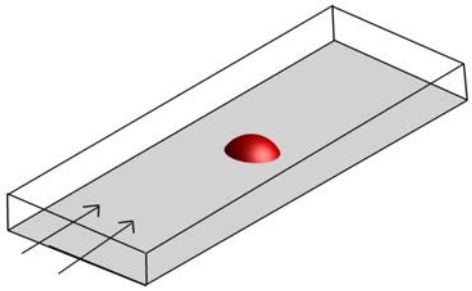

Figure 1: Schematic diagram of micro-channel geometry. The red surface represents a thrombus on the lower surface of the channel. Arrows designate the flow through the channel.

The shape is idealized as a partial protrusion of a sphere (in 3D) or a circle (in 2D) through the centreline of the lower wall of the channel, as illustrated in figure 1. The protrusion is defined as a ratio of thrombus height H_T to the radius of the sphere defining it r_T. This ratio was fixed at 0.25 in this study to maintain geometric similarity.

The micro-slide channel is a long rectangular duct and the thrombus is considered to be far away from entrance effects. The channel aspect ratio $AR = W / H$ based on the channel width W and height H was set at 10 to match the experimental conditions.

This geometry produces a flow field which is three-dimensional. Two-dimensional approximations of this system result in more dramatic changes in area, and as a result, an over-estimation of changes in velocity and pressure. A Newtonian fluid solver is considered to be an acceptable model for all the simulations in this study as the flow conditions are steady state (Rodkiewicz et al., 1990).

In studies of vascular flow, shear forces are considered to be an important physical stimulus both on blood cells and the vessel walls. Shear rate is commonly used instead of shear force. Under the Newtonian assumption, the shear rate is directly proportional to the shear force τ through the dynamic viscosity.

The shear rate at the walls for these perfusion channel geometries is commonly calculated using two-dimensional Poiseuille flow conditions. This produces a Reynolds number based on the wall (maximum) shear, defined as

$$Re = \frac{\gamma_{wall} H^2}{4\upsilon}.$$

This definition for Reynolds number and shear rate was derived based on the 2D Poisuille flow assumption. As the system has a limited aspect ratio a more sophisticated definition is required. In this case the solution of laminar duct flow (Appendix A) is used to calculate a maximum shear, which occurs at the channel wall centreline. This is consistent with the position where the thrombus occurs in the experimental studies.

The peak Poiseuille shear rate γ_{wall} forms the basis for a nondimensionalization of the shear rate in this problem. A non-dimensional shear rate χ is defined as the ratio of the local shear rate to the Poiseuille shear rate,

$$\chi = \frac{\gamma}{\gamma_{wall}}$$

The thrombus height (H_T) is considered the characteristic dimension for this study; consequently it is non-dimensionalized by the channel height (H), providing a height ratio,

$$h_t = \frac{H_T}{H}.$$

Parameter space

A single Reynolds number (Re = 6.84) is considered in this study, which matches the shear rate (γ = 1800) measured in the experimental studies. A range of 21 cases were investigated between $0.02 \leq h_t \leq 0.8$. Lagrangian particle tracking (Sheard et al. 2007) was conducted in each case.

NUMERICAL METHODOLOGY

A spectral-element method forms the basis of the spatial discretization technique for this study. The formulation is a Newtonian flow solver (Karniadakis and Sherwin, 1999). The two-dimensional mesh consists of quadrilateral macro elements with a tensor product of Lagrangian polynomials as the shape functions evaluated at nodal points.

While the geometry is axisymmetric, the flow is not. As a consequence a formulation of the spectral-element/Fourier (SEF) technique is used. An SEF technique uses a Fourier expansion to discretize the flow in the third dimension. Blackburn and Sherwin (2004) described a technique for an azimuthal expansion for the third dimension; in addition the change of variable imposed in this method decouples the Fourier modes allowing efficient parallelization. Significantly this solver permits flow through the axis of the expansion. The result is a solver which achieves spectral convergence through two independent control methods, the number of Fourier modes used and the number of nodes evaluated for the Lagrangian polynomials.

While the flow asymptotes to a steady state, the solution is obtained by evolving the time-dependent incompressible Navier-Stokes equations,

$$\left(\frac{\partial \mathbf{u}}{\partial t} + \mathbf{u}\cdot\nabla\mathbf{u}\right) = -\nabla P + \upsilon\nabla^2\mathbf{u},$$

$$\nabla\cdot\mathbf{u} = 0,$$

from a non-physical initial condition. The time stepping scheme converges to the steady state solution in this problem via a third-order operator splitting scheme. It is noted that for steady-state solutions, the time splitting errors are zero for any stable time-step (Karniadakis et al., 1991).

Grid Geometry

The grid geometry was specified to align with the geometry as considered in the model description section. The z axis passes vertically through the centre of the thrombus, and the (radial) edge was set such that the mesh "touched" the micro-channel wall at its extremity. This imposes a mesh radial length (L) on height ratio (H) which is half of the aspect ratio, AR. The mesh, shown in figure 2 is a meridonal half plane, on which the spectral-element grid is defined. This matching of the radial dimension to the channel width was considered a sufficient domain size for the Reynolds number considered. Care was taken to minimize the skewing of elements in all cases. The number of macro elements in the grid ranged between 120 and 170 depending on the height ratio h_T. Elements employing a polynomial degree of 10 were used and 40 Fourier modes were employed, which resolved the flow within numerical precision error for the technique. Resolution studies were conducted both in space and time to ensure consistency and accuracy of the solution.

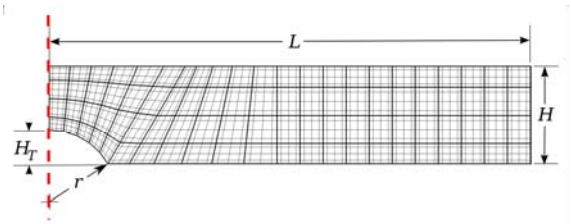

Figure 2: Mesh Geometry of the spectral element grid. A single r-z plane representing the axisymmetric geometry. The dashed red line represents the z-axis (axis of revolution). Bold lines mark the spectral-elements and faint lines represent the nodal evaluation points. The number of nodes per element depicted was reduced for clarity.

POST PROCESSING TECHNIQUES

Particle Tracking

In addition to solving the flow field, a number of passive particles are introduced. These particles simulate the flow of platelets through the channel, thus capturing the spatial and temporal history of shear rate on the platelets. The method, a variation that proposed by Coppola et al. (2001), uses the high order accuracy of both the Fourier modes and Lagrangian polynomials. A fourth order Runge-Kutta technique is used to advance the particles within elements, and linear sub-steps are employed to traverse element interfaces. Particle tracking provides high-order space-time histories of platelet motion under the assumption that the platelets do not disturb the flow field. As the flow-field converges to a steady state solution the particle tracking algorithm is employed on a frozen base flow solution, where only the particle tracks are evolved and not the flow field. This allows rapid and efficient computation of the particle tracks.

Shear rate calculation in three dimensions

In a two-dimensional channel, the shear rate for Poiseuille flow reduces to

$$\dot{\gamma} = \frac{8U_{peak}.z}{h}, \qquad -\frac{H}{2} \le z \le \frac{H}{2},$$

where H is defined as the channel height and U_{Peak} the peak flow velocity. The simplicity of this equation is due to the steady state flow which is constant in the flow direction. Fluidic strain rate and shear rate are analogous to strain and shear in solid mechanics. Most importantly, given a set of spatial derivatives (strains and shears), at any point principal strains and shears may be found. Given the unknown relationship for shear/strain interaction for platelet adherence and activation, the principal shears and strains are considered the relevant parameters.

The principal strains λ can be defined as the eigenvalues of the strain rate tensor S, written in Cartesian tensor notation as

$$S = 0.5\left(\frac{\partial u_j}{\partial x_i} + \frac{\partial u_i}{\partial x_j}\right).$$

The principal shear is the difference between the maximum and minimum principal strains,

$$\gamma = \lambda_{\max} - \lambda_{\min}.$$

Calculated in this fashion, only the magnitude of the shear rate is determined. An additional level of complexity is introduced due to the solver formulation using a cylindrical coordinate system. The shear rate is solved using the cylindrical velocity gradient tensor V (Appendix B) which is used to calculate the strain tensor as,

$$S = 0.5\left(V + V^T\right),$$

which can be solved for its eigenvalues and consequently the shear rate. It is noted that at the axis, the solution is singular despite the existence of a finite strain at that point. This has no effect on the solver due the formulation of Blackburn and Sherwin (2004). Thus the principal shear rate may be calculated at all points in the domain with the exception of the axis (r=0).

RESULTS

Peak shear rate for an increasing thrombus size

The peak shear rate was calculated by finding the maximum shear rate at the nodal evaluation points. No extrapolation or high order interpolation was used. In all cases the shear maxima were located on the surface of the thrombus. The shear rate minima has not been displayed, this is as large number of minima are present, a result off the shear rate at the centreline of a Poiseuile flow, the imposed boundary conditions, is zero. Local minima and maxima occur at the leading and trailing stagnation points of the thrombus. These occur along the thrombus centreline, at the intersection of the thrombus and the surface.

Figure 3 shows the peak shear rate which was observed through the study. The figure shows the shear rate peaking as h_t approaches zero, suggesting that a single platelet adhered to the wall generates the maximum shear rate increase of 280% from the Poiseulle inlet conditions at the smallest thrombus size considered. The peak shear rate decreases with increasing h_T to h_T = 0.5, before again gradually increasing.

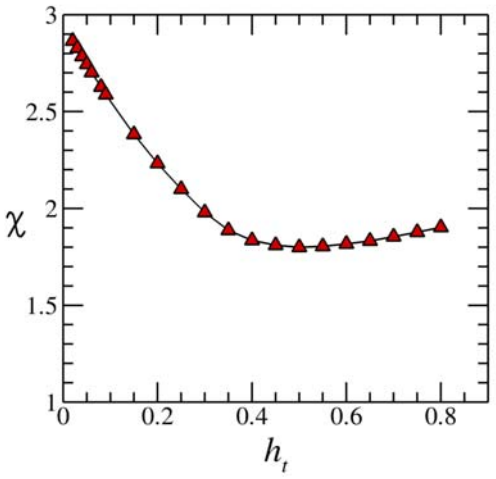

Figure 3: The maxima of non dimensional shear rate over the entire mesh volume versus the nondimensional thrombosis height.

Peak shear rate location and structure

We observed that the shear rate maximum was always occurring on the surface of the thrombus. This is consistent with steady Poiseuille flow where the maximum shear rate occurs on the walls. The contour plots of figure 4 illustrate the behaviour of the forces as the height of the bump is increased. Figure 4(a) demonstrates a near symmetry in the flow direction. This symmetry is consistent with a Stokesian flow locally around the bump. The Reynolds number of the channel Re=6.84 is well above Stokes flow conditions. However, a Reynolds number Re_T based on the thrombus height H_T where the velocity U_{Peak-} is defined as the peak inlet velocity, yields a range of $0.12 \leq Re_T \leq 5.84$ where the lower end is consistent with creeping flow regime $Re << 1$.

The effect of convection can be seen though the movement of the peak forward on the centreline, away from a Stokesian symmetry in figure 4b. The most interesting behaviour is the transition from a single shear rate peak to dual peaks in figures 4c and 4d. This is seen to be of significant interest, as it suggests a change in the behaviour and pattern of thrombus growth. Platelets experiencing the peak shear will no longer be passing over the top, rather around the side of the thrombus.

Figure 5 shows a consequence of the transition to dual peaks. The position of peak shear always occurs on the thrombus, thus we can define this in terms of the height above the surface. Before the transition to dual peaks the shear rate maxima height increases linearly with the height increase. At transition h_T =0.3 the height of maximum shear plateaus rapidly.

Platelet shear rate history via particle tracking

Multiple particle tracks were examined for all computed flow fields. A selection of the data is presented in this paper. Platelets were introduced at approximately one platelet diameter away from the wall (2μm) equating to 1% of the domain height.

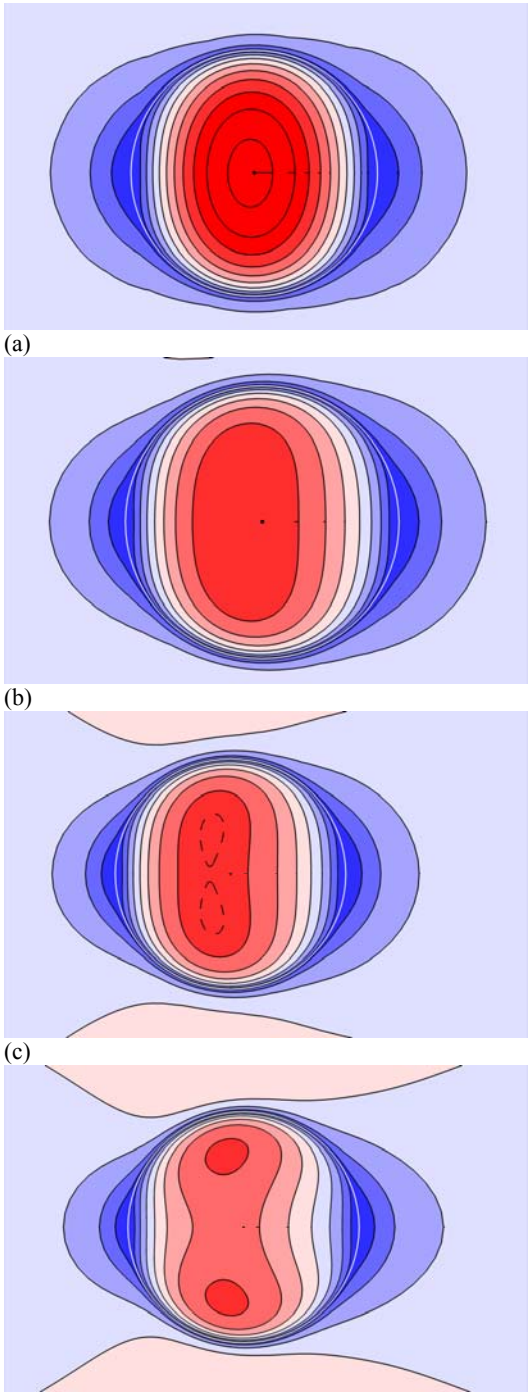

Figure 4: Contour plots of shear rate at even intervals. Contours are on the lower surface (including the thrombus) with flow travelling left to right across the page. The white ring represents the edge of the thrombus. In each case the size has been scaled for clarity. Doted contour is a half sized interval to visualize the peaks clearly. White contour colouring represents χ = 1. Blue and red contours represents negative and positive variations from that level. The following are the associated cases for each contour: (a) h_t = 0.09., (b) h_t = 0.25. (c) h_t = 0.3.. (d) h_t = *0.8.*

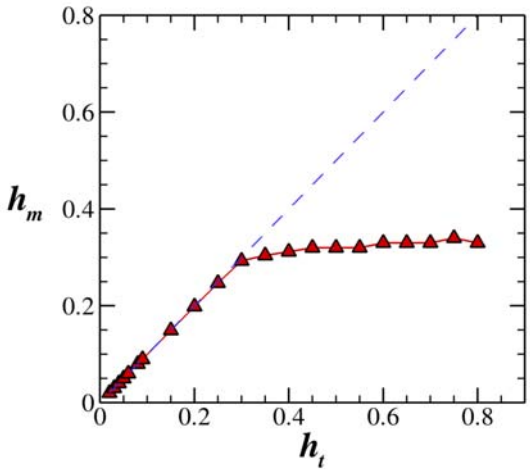

Figure 5: Location of maximum shear (z-displacement). The x-axis represents the nondimensionalised height of the thrombus, the vertical axis represents the scaled height of maximum shear h_M. The dashed line represents the case where $h_M = h_t$.

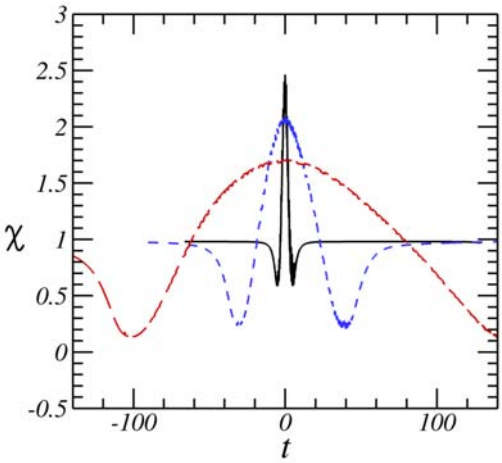

Figure 6: Temporal variation of shear along particle tracks. Nondimensional shear rate χ is plotted against time. Time is normalized by a shift such that the peah shear occurs at $t = 0$. The black solid track represents the case $h_t = 0.09$, the blue short dashes represent case $h_t = 0.25$ and the red long dashes represent $h_t = 0.5$

Figure 6 shows the variation of shear in terms of time history for each of the flows. A selected particle track at the axis is shown for 3 cases. The location and magnitude of the shear rate peak in the particle tracks is consistent with that recorded from the calculations over the domain. It can be seen immediately that for small thrombus sizes the temporal rate change of shear rate is extremely large compared with the larger thrombus sizes. This very large scale in differences may point to the potential cause of stability in thrombus size *in-vivo*.

DISCUSSION

The introduction of a thrombus into an *in-vitro* geometry is shown to produce large variations in shear local to the thrombus. As activation/adherence of the platelets is believed to be shear dependent, the significant decay in peak shear as the thrombus increases in size is significant. When considering this fact, and relating it to an *in-vivo* geometry, the effect of vessel occlusion is not modelled. Even for the largest sized thrombus in this case the occlusion of the geometry is relatively small, (<15 %).

The change in the behaviour of shear forces around a thrombus as it grows is the significant outcome of this study. The transition from a near Stokesian solution to a solution affected by convection (from figure 4a to 4b), does not significantly affect the paths the platelets experiencing maximum shear. However, the transition to twin peaks of shear (figure 4b to 4d) moves the peak shear away from the centreline. As a result, platelets which move around rather over the top of the thrombus will experience peak shear. We hypothesise that this transition will trigger a change in pattern in platelet activation and adherence, leading to a change in thrombus shape.

From the observations of both the peak shear rate and the pattern of shear observed at the thrombus, there is a number of contributing effects to the location and level of peak shear. The curvature of the thrombus regulates shear: as the curvature increases so too does the shear. The second effect is the relative size in the channel: as the thrombus increases in size, it moves through the parabolic profile. This is the effect which leads to the transition from a single shear peak to the twin peaks system.

A combination of these two effects explains the gradual increase at $h_t \geq 0.5$. A decrease in curvature is offset as the thrombus grows into the high shear region on the opposing wall. A more dramatic increase in shear would be expected from lower aspect ratios observed in *in-vivo* geometries when compared with the *in-vitro* geometry. This is due to the higher occlusion which happens in lower aspect ratio geometries.

One key result is obtained from the particle tracks. As the thrombus size increases, the temporal variation in shear decreases significantly. This decrease is non-linear with respect to thrombus size. This is an interesting result as it illustrates a connection between the earlier work of Goncalves et al. (2005) and the recent work of Nesbitt et al. (2009). The spatial shear rate "micro gradients" observed in Nesbitt et al. (2009) may not directly cause thrombus growth, but rather be a limited form of the temporal shear variation observed in Goncalves et al. (2005). Additionally it is a potential explanation of thrombus growth in vessels where shear is much lower than the peak through the entire vascular system, illustrating that how rapidly the shear rate varies in time may be as important as the peak shear itself. This reduction in temporal shear change with increasing thrombus size may explain the stability of thrombus *in-vivo*. At this time it is unclear whether spatial or temporal gradients drive platelet activation, however, evidence presented in this paper suggests that temporal gradients may contribute more than shown in Nesbitt et al. (2009).

CONCLUSION

A numerical investigation employing three-dimensional direct numerical simulations examines the flow past an axisymmetric thrombosis in an experimental geometry. For a geometrically similar thrombosis, as the size changes within the channel, a significant variation in peak shear rate occurs. An initial decrease in shear from the

maximum occurs as h_t increases from 0 to 0.5. Following that there is a gradual increase as the thrombosis grows towards the opposing wall. This growth sees transitions in the behaviour of shear rate in the vicinity of the thrombus. A significant transition occurs where the peak shear moves from one to two peak locations on the thrombosis. This transition accompanied by a plateau of the peak shear location in the vertical direction. As platelets are shear activated this represents a significant change in the activation pattern and resulting growth of the thrombus. Additionally, a transition to creeping flow conditions in the vicinity of the thrombus as h_T approaches zero represents a limiting factor for the potential increase in shear with decreasing thrombus size. This increase is limited by the "single platelet" clot, which the smallest case considered is a close approximation to.

Passive particle tracking verified that high temporal gradients in shear rate occur in the proximity of the thrombus. It is noted that even though the difference between the minimum and maximum shear rate increase as $h_t \geq 0.5$ The shear rate change (temporally) on a platelet is still decreasing. Further work is required to quantify whether spatial or temporal gradients are the dominant criterion for platelet activation.

ACKNOWLEDGEMENTS

The authors would like to thank Monash eResearch Centre (MeRC) and Monash ITS research support services for providing access to the Monash Campus Grid computational facilities use to complete this study. C.J.B would also like to thank MeRC for the HPC scholarship and the Department of Mechanical and Aerospace Engineering, Monash University for providing support for participation in the conference.

REFERENCES

BLACKBURN, H. M. and SHERWIN, S. J., (2004). "Formulation of a Galerkin spectral element–Fourier method for three-dimensional incompressible flows in cylindrical geometries." *J. Comput. Phys.* 197(2): 759-778.

CARO, C. G., FITZ-GERALD, J. M. and SCHROTER, R. C., (1969). "Arterial wall shear and distribution of early atheroma in man." *Nature* 223: 1159-1161.

COPPOLA, G., SHERWIN, S. J. and PEIRO, J., (2001). "Nonlinear particle tracking for high-order elements." *J. Comput. Phys.* 172(1): 356-386.

DOPHEIDE, S. M., MAXWELL, M. J. and JACKSON, S. P., (2002). "Shear-dependent tether formation during platelet translocation on von Willebrand factor." *Blood* 99(1): 159.

EISENBERG, P. R. and GHIGLIOTTI, G., (1999). "Platelet-dependent and procoagulant mechanisms in arterial thrombosis." *Int. J. Cardiol* 68: 3-10.

FOURAS, A., (2008). Personal communication.

GONCALVES, I., NESBITT, W. S., YUAN, Y. and JACKSON, S. P., (2005). "Importance of Temporal flow Gradients and Integrin $\alpha_{IIb}\beta_3$ Mechanotransduction for Shear Activation of Platelets " J. Biol. Chem. 280(15): 15430-15437.

HATHCOCK, J. J., (2006). "Flow effects on coagulation and thrombosis." *Arterioscler. Thromb. Vasc. Biol.* 26(8): 1729.

KARNIADAKIS, G., ORSZAG, S. and ISRAELI, M., (1991). "High-order splitting methods for the incompressible Navier-Stokes equations." *J. Comput.. Phys.* 97: 414-443.

KARNIADAKIS, G. and SHERWIN, S. J., (1999). "Spectral/hp element methods for CFD", Oxford University Press, USA.

KROLL, M. H., HELLUMS, J. D., MCINTIRE, L. V., SCHAFER, A. I. and MOAKE, J. L., (1996). "Platelets and shear stress." *Blood* 88(5): 1525.

MAXWELL, M. J., WESTEIN, E., NESBITT, W. S., GIULIANO, S., DOPHEIDE, S. M. and JACKSON, S. P., (2007). "Identification of a 2-stage platelet aggregation process mediating shear-dependent thrombus formation." *Blood* 109(2): 566.

NESBITT, W. S., WESTEIN, E., TOVAR-LOPEZ, F. J., TOLOUEI, E., MITCHELL, A., FU, J., CARBERRY, J., FOURAS, A. and JACKSON, S. P., (2009). "A shear gradient–dependent platelet aggregation mechanism drives thrombus formation." *Nature Medicine* 15(6): 665-673.

RODKIEWICZ, C. M., SINHA, P. and KENNEDY, J. S., (1990). "On the application of a constitutive equation for whole human blood." *J .Biomech. Eng.* 112: 198.

SHEARD, G. J., LEWEKE, T., THOMPSON, M. C. and HOURIGAN, K., (2007). "Flow around an impulsively arrested circular cylinder." *Phys .Fluids* 19: 083601.

TOLOUEI, E., NESBITT, W. S., FOURAS, A. and CARBERRY, J., (2008). "A High Spatial Method to Determine Three-Dimensional Velocity Gradient Tensor using Micro Particle Image Velocimetry." *In Proc of 14th Int. Symp. on Applications of Laser Techniques to Fluid Mechanics,* Lisbon, Portugal, 7-10 July

WHITE, F. M. (1991). "Viscous fluid flow", McGraw-Hill New York.

WOOTTON, D. M. and KU, D. N., (1999). "Fluid mechanics of vascular systems, diseases, and thrombosis." *Annu. Rev. Biomed. Eng* 1(1): 299-329

APPENDIX A: LAMINAR DUCT FLOW

The boundary conditions for the inflow-outflow boundary in the study were represented by an analytic solution to rectangular duct flow (White 1991). This equation,

$$u(y,z) = \frac{48Q}{4\pi^3 ab} \times \frac{1}{1 - \frac{192a}{\pi^5 b} \sum_{i=1,3,5..}^{\infty} \frac{1}{i^5} \tanh\left(\frac{i\pi b}{2a}\right)} \times \text{ and,}$$

$$\sum_{i=1,3,5...}^{\infty} \frac{(-1)^{(i-1)/2}}{i^3} \left[1 - \frac{\cosh(i\pi z/2a)}{\cosh(i\pi b/2a}\right]$$

is a reduction of the system which defines the velocity in terms of channel size a flow rate. It is convenient as it eliminates viscosity from the solution. The equation is imposed on a domain where $-a \leq y \leq a$, $-b \leq z \leq b$ and Q is the volumetric flow rate through the channel.

APPENDIX B: CYLINDRICAL VELOCITY GRADIENT TENSOR

$$V = \begin{bmatrix} \frac{\partial U_z}{\partial z} & \frac{\partial U_z}{\partial r} & \frac{\partial U_z}{\partial \theta}\frac{1}{r} \\ \frac{\partial U_r}{\partial z} & \frac{\partial U_r}{\partial r} & \frac{\partial U_r}{\partial \theta}\frac{1}{r} \\ \frac{\partial U_\theta}{\partial z} & \frac{\partial U_\theta}{\partial r} - \frac{U_\theta}{r} & \left(\frac{\partial U_\theta}{\partial \theta} + U_r\right)\frac{1}{r} \end{bmatrix}$$